PNAS RESEARCH ARTICLE | GENETICS OPEN ACCESS

Improved synapsis dynamics accompany meiotic stability in *Arabidopsis arenosa* autotetraploids

Adrián Gonzalo[a,1], Aditya Nayak[a], and Kirsten Bomblies[a,1]

Edited by Michael Lichten, National Institutes of Health, Bethesda, MD; received October 2, 2024; accepted March 31, 2025

During meiosis, the correct pairing, synapsis, and recombination of homologous chromosome pairs is critical for fertility of sexual eukaryotes. These processes are challenged in polyploids, which possess additional copies of each chromosome. Polyploidy thus provides a unique context to study how evolution can modify meiotic programs in response to challenges. We previously observed that in newly formed (neo-)polyploids of *Arabidopsis arenosa*, synapsis defects precede chromosomes associating in aberrant multivalent and univalent configurations. Here, we study synapsis dynamics in genotypes with varying levels of meiotic stability to ask whether efficient synaptic progression is a key component of evolving stable tetraploid meiosis. We develop a method to quantify synapsis dynamics using the progression of foci of the pro-crossover factor HEI10 as a reference. HEI10 initially appears at many small foci before accumulating only at crossover sites. In diploids, this transition begins while significant asynapsis is still present, though it quickly declines as HEI10 accumulates at fewer foci. In neo-tetraploids, suboptimal elongation of synaptic initiation sites and stalled synapsis, perhaps due to defective pairing, occurs before the onset of HEI10 accumulation. In established tetraploids, HEI10 accumulation begins only when synapsis is near complete, suggesting enhanced HEI10/synapsis codynamics (even compared to diploids). Hybrids generated by crossing neo- and established tetraploids exhibit intermediate phenotypes. We find the extent of asynapsis correlates positively with crossover numbers, and the frequency of multivalents and univalents, which can disturb chromosome segregation. Our work supports the hypothesis that improving the efficiency of synapsis is important for evolving polyploid meiotic stability.

polyploidy | meiosis | synapsis | recombination

Significance

Meiosis is a special cell division essential for fertility in most eukaryotes. During meiosis, homologous chromosomes are separated to give rise to haploid spores or gametes. Key events such as pairing, synapsis, and crossing-over can be perturbed by genome duplication (polyploidy). What goes wrong, and how polyploids evolve to fix it, remains unclear. Leveraging the dynamics of the pro-crossover factor HEI10 as a "developmental clock" in *Arabidopsis arenosa*, we found synapsis is severely compromised in neo-tetraploids, while in established ones it is more efficient even than diploids. The extent of synaptic defects correlated with meiotic instability, showing that improving synapsis is important for the evolution of meiotic stability in polyploids.

Meiosis is a specialized cell division essential for fertility of sexual eukaryotes. Meiosis halves the chromosome complement through two rounds of segregation, producing haploid cells (spores or gametes). Crossovers among homologs occur during meiosis, which have a dual consequence of generating new trait combinations, while also holding homologous chromosomes in tight apposition to ensure proper chromosome segregation—and thus fertility—in meiosis I (1). In polyploids, whole genome duplication leads to a genome with more than the usual two copies of each chromosome, which can disrupt key meiotic processes and compromise segregation (2). Understanding which processes are perturbed by genome duplication, and how they are adjusted in evolved polyploids, can provide novel insights into meiosis and its evolution (3), as well as help us understand how polyploids reestablish meiotic stability.

In diploids, the proper number and patterning of crossovers is regulated by a meiotic program that ensures pair-wise interactions between homologs (forming bivalents) during prophase I of meiosis. Recombination begins with the formation of DNA double-strand breaks (DSBs) (4), which are subsequently processed in the context of linear proteinaceous axes that form along the length of each homolog (5). DSBs are typically required for subsequent homolog coalignment, and polymerization of the synaptonemal complex during zygotene (6). The synaptonemal complex holds homologs in close alignment as recombination events mature, and its formation coincides with the partial removal of some axis proteins, such as ASYNAPSIS1 (ASY1) in plants (7, 8). The synaptonemal complex acts as a platform for recombination proteins, including the dosage-sensitive Human Enhancer of Invasion-10 (HEI10), which progresses from many dispersed weak foci in early pachytene to fewer bright foci that mark crossover sites in late pachytene (9–13). This process of HEI10 accumulation has been modeled based on data from *Arabidopsis thaliana* and *Caenorhabditis elegans* to follow the biophysics of a "coarsening" process that has been proposed to explain crossover patterning (14, 15). However, this model is debated, as it implies that crossover designation occurs later than proposed in well-supported models from budding yeast and *Sordaria* (16, 17). Regardless of the role

Author affiliations: [a]Department of Biology, Institute of Molecular Plant Biology, ETH Zürich, Zürich 8093, Switzerland

Author contributions: A.G. and K.B. designed research; A.G. performed research; A.N. contributed new reagents/analytic tools; A.G. analyzed data; and A.G. and K.B. wrote the paper.

The authors declare no competing interest.

This article is a PNAS Direct Submission.

[1]To whom correspondence may be addressed. Email: adrian.gonzalo@biol.ethz.ch or kirsten.bomblies@biol.ethz.ch.

This article contains supporting information online at https://www.pnas.org/lookup/suppl/doi:10.1073/pnas.2420115122/-/DCSupplemental.

Published May 7, 2025.

of HEI10 accumulation, defective synaptonemal complex formation is known to cause abnormal crossover numbers and patterns in some species, including *Arabidopsis* (18–21), though how exactly this links to the HEI10 "coarsening" process remains debated.

The processes of both synapsis and HEI10 accumulation are conserved across eukaryotic kingdoms (10, 11, 16, 22–24). However, it is not known how they might be affected by whole genome duplication or how they might evolve in response. In our previous work on natural autotetraploid *A. arenosa* [which arose from a single within-species whole genome duplication about 30,000 generations ago (25)] we found that high frequency of meiotic aberrations leading to formation of multivalents and/or univalents (instead of bivalents) in new polyploids is accompanied by defects in synapsis and crossover patterning (26). Meiotically stable established tetraploids, in contrast, which have almost exclusively bivalents at metaphase I, not only evolved improved crossover patterning, but also recovered full synapsis (26). It remained unknown at what stage synapsis becomes defective in neo-polyploids, whether it is stalled or merely slow, to what extent established tetraploid synapsis is enhanced, or whether the synaptic defects in neo-polyploids relate directly to defects in crossover patterning. We explore this here.

To clarify when and how synapsis becomes defective in neo-tetraploids, and whether evolved tetraploids have more efficient synapsis to attenuate this problem, we studied the codynamics of synapsis and HEI10 progression in diploid, neo-tetraploid, and established tetraploid *A. arenosa*. Quantifying these dynamics would ideally require live imaging (27), but this is limited to a few model species. Therefore, we developed a quantitative framework to assess synapsis dynamics in male meiocytes. We found that in neo-tetraploids synapsis is fully stalled already in prophase I, not just slow, and that this is associated with defects in chromosome coalignment. Though synaptic initiation appears normal in the neo-tetraploids, the synaptonemal complex seems to be unable to efficiently elongate from the initial sites. These defects correlate with increased crossover rates, suggesting crossover patterning issues, which in turn may cause the observed extensive multivalent and univalent formation. In contrast, established tetraploids exhibit more efficient synapsis, even surpassing diploids, suggesting that synapsis improvements contributed to meiotic stabilization and improved crossover regulation.

Results

Crossover Number and Meiotic Stabilities of all Genotypes at Metaphase I. To explore the link between prophase I defects and meiotic instability in metaphase I, we quantified meiotic features in natural diploids (2X), neo-tetraploid lines created by colchicine treatment in the lab (NEO-4X; see *Material and Methods*), evolved tetraploids (EST-4X), and first-generation hybrids (HYB-4X) from crosses between EST-4X and NEO-4X (*SI Appendix*, Fig. S1). We analyzed metaphase I and diakinesis spreads (Fig. 1 *A* and *B*). As previously reported (26, 28), 2X showed full meiotic stability with all chromosome pairs forming bivalents. EST-4X formed on average less than 1 quadrivalent per cell (Fig. 1*C*) and very rarely univalents (0.1 per cell; Fig. 1*D*). HYB-4X had significantly more quadrivalents than EST-4X (Fig. 1*C*), but a similarly low number of univalents (Fig. 1*D*). In contrast, NEO-4X formed significantly more quadrivalents (3.0 ± 1.9 per cell, $P < 0.0041$, Fig. 1*C*) and also more univalents (0.9 ± 1.4 per cell, $P > 0.0031$, Fig. 1*D*).

Because the frequency of quadrivalents should be positively (and univalents negatively) correlated with crossover frequency (29–31), we also measured crossover number in 2X, NEO-4X, HYB-4X, and EST-4X by immunostaining for HEI10, which in late prophase I stages of diplotene and diakinesis forms discrete foci at Class I crossover sites (32) (Fig. 1*B*). Consistent with previous reports (26) we scored ~10 HEI10 foci per cell in 2X, about 22 in NEO-4X and 17 in EST-4X. HYB-4X had an intermediate number (about 18 foci) between its two parent genotypes (Fig. 1*E*), suggesting crossover number, like multivalent frequency, has a semidominant genetic basis.

Quantification of HEI10 Accumulation Enables Modeling of Synapsis Progression. To obtain a detailed picture of prophase I dynamics in the different tetraploid materials, we developed a quantitative framework by exploiting observable changes in HEI10 localization during pachytene as a "developmental clock." HEI10 signal typically transitions from a very dispersed pattern of numerous weak foci in early pachytene, to a few bright and enlarged foci that mark the position of crossovers in late pachytene (10, 14, 22–24). We will refer to this dynamic process as "HEI10 accumulation." We used HEI10 accumulation as a quantitative proxy for the developmental progression of meiosis to study the dynamics of other concomitant events, mainly synapsis.

We imaged male meiocytes in the prophase I stages of zygotene and pachytene in a set of 17 plants (*SI Appendix*, Fig. S1), including 2X (4 plants), NEO-4X (6 plants), HYB-4X (3 plants), and EST-4X (4 plants) using Structured Illumination Microscopy (SIM). We immunolocalized three meiotic proteins (Fig. 2*A*): ZYP1 (the transverse filament of the synaptonemal complex, which marks synapsed axes), ASY1 (an axis component largely removed upon synapsis, thus serving as a marker for unsynapsed chromosomes), and HEI10 (to mark intermediates at different stages of the recombination process). Prior to image analysis, we verified that these three antibodies specifically stain meiotic cells; as expected, only a dim background signal was detected upon overexposure in somatic cells (*SI Appendix*, Fig. S2 *A* and *D*).

Using a Fiji macro (see *Material and Methods*; Fig. 2*A* and *SI Appendix*, Figs. S2*B* and S13), we quantified HEI10 signal distribution while preventing bias from human decisions through particle analysis of HEI10 foci. The "HEI10 accumulation level" was calculated on each cell as the percentage of HEI10 signal intensity in the most relatively prominent foci compared to the total HEI10 signal intensity in that cell (Fig. 2*A* and *SI Appendix*, Figs. S2 *B* and *C* and S13). We defined "prominent foci" vs. "total signal" using two different automated detection thresholds (Fig. 2*A* and *SI Appendix*, Figs. S2 *B* and *C* and S14 see also *Material and Methods*). Each image serves as a "snapshot" of a dynamic process, showing diverse HEI10 accumulation levels across different cells (Figs. 2*A* and 3*A*), from low (where prominent foci account for a small share of total HEI10 signal intensity; Fig. 2*A*) to high (where most total HEI10 signal is concentrated in prominent foci, presumably marking crossover sites; Fig. 2*A*).

To assess the potential effect of background signal on HEI10 accumulation, we measured somatic and meiotic leptotene cells, where HEI10 accumulation should be zero (*SI Appendix*, Fig. S2*D*). Since our image analysis method is based on relative intensities (as described in *Material and Methods* and *SI Appendix*, *Supporting Information Text*), some background unspecific fluorescent signals can be more relatively intense than others. This means that somatic cells, though lacking true HEI10 signal, can register as having a certain signal accumulation level. Somatic and early meiotic cells registered an average of 7% HEI10 accumulation, with a maximum of 12% (*SI Appendix*, Fig. S2*E*). As we observed somatic cells with accumulation levels of up to 12% whereas some pachytene cells (fully synapsed) may show levels of 3%, we concluded that those low levels of HEI10 accumulation

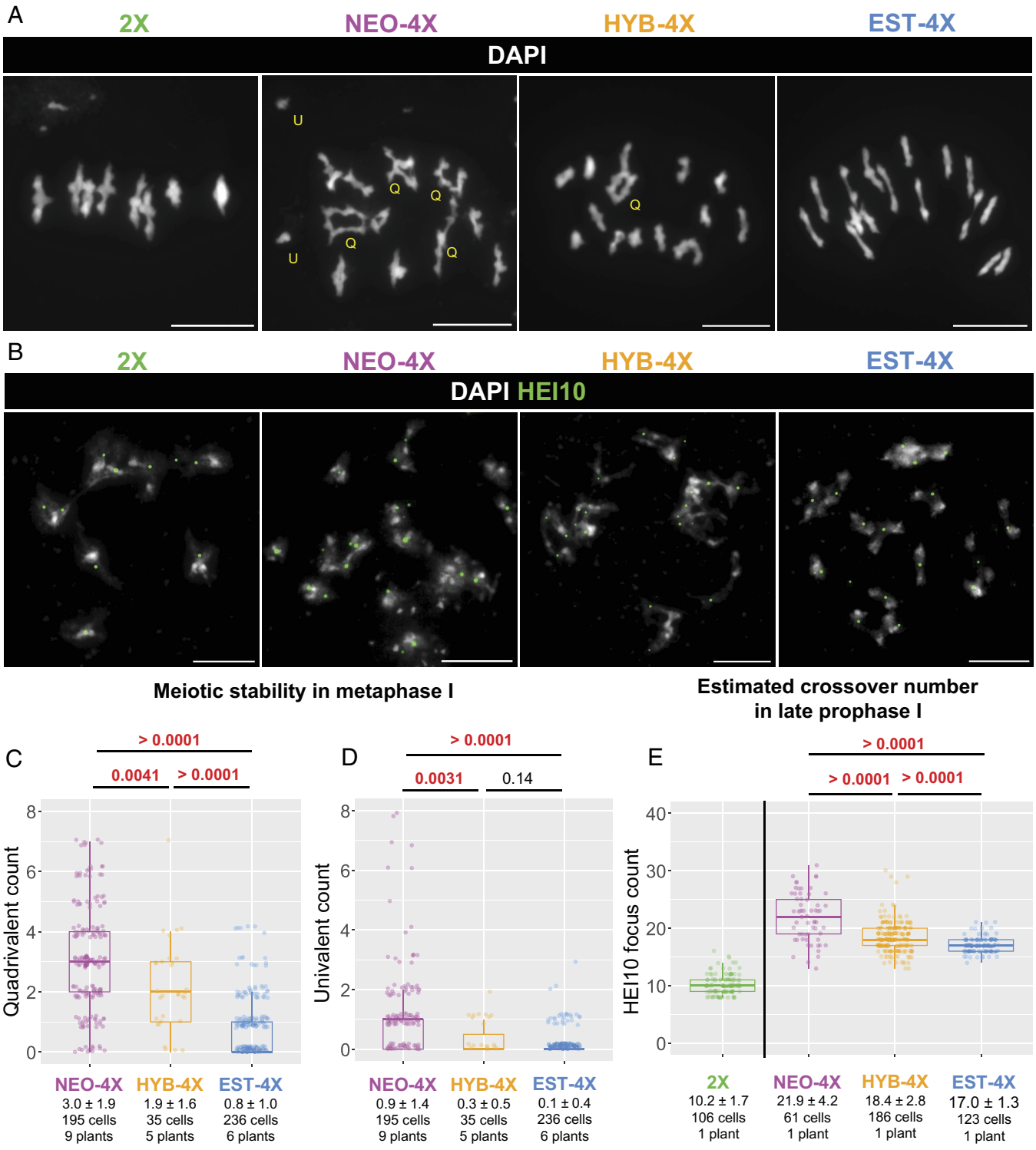

Fig. 1. Crossover number and meiotic stability in different tetraploid populations. (Scale bar, 10 μm.) (*A*) Examples of metaphase I spreads from all genotypes. Yellow Q, T, and U, mark examples of quadrivalents, trivalents, and univalents, respectively. (*B*) Examples of diakinesis cells with HEI10 immunostaining to detect crossovers. (*C* and *D*) Box plots of quadrivalent (*C*) and univalent (*D*) counts per cell. (*E*) HEI10 foci count in late prophase I (diplotene plus pachytene) cells. For (*C*), (*D*), and (*E*), population name, mean ± SD, and sample size. *P*-values are indicated on top of the plots for each comparison (according to Wald's test on negative binomial-GLMM, Poisson-GLMM coefficients for (*C*) and (*D*); and Dunnett's test for (*E*). Significant *P*-values are highlighted in red.

do not inform on the developmental stage of meiotic cells. Therefore, we excluded cells with HEI10 accumulation levels below 12% from further analyses, as these values might be indistinguishable from background. This resulted in a final dataset of 523 imaged meiocytes from all genotypes (2X: 125 cells from 4 plants; NEO-4X: 172 cells from 6 plants; HYB-4X: 134 cells from 3 plants; EST-4X: 94 cells from 4 plants). To quantify synapsis levels, we used the ASY1 3D length (in μm) as a negative proxy for synapsis completion. Unfortunately, the punctate pattern of ZYP1 immunostaining precluded reliable automated measurement of its 3D length (*SI Appendix*, Fig. S2*F*).

Next, we fitted a Gamma-Generalized Linear Mixed Model (Gamma-GLMM; see *Material and Methods* and *SI Appendix*) using HEI10 accumulation level and genotype as predictors

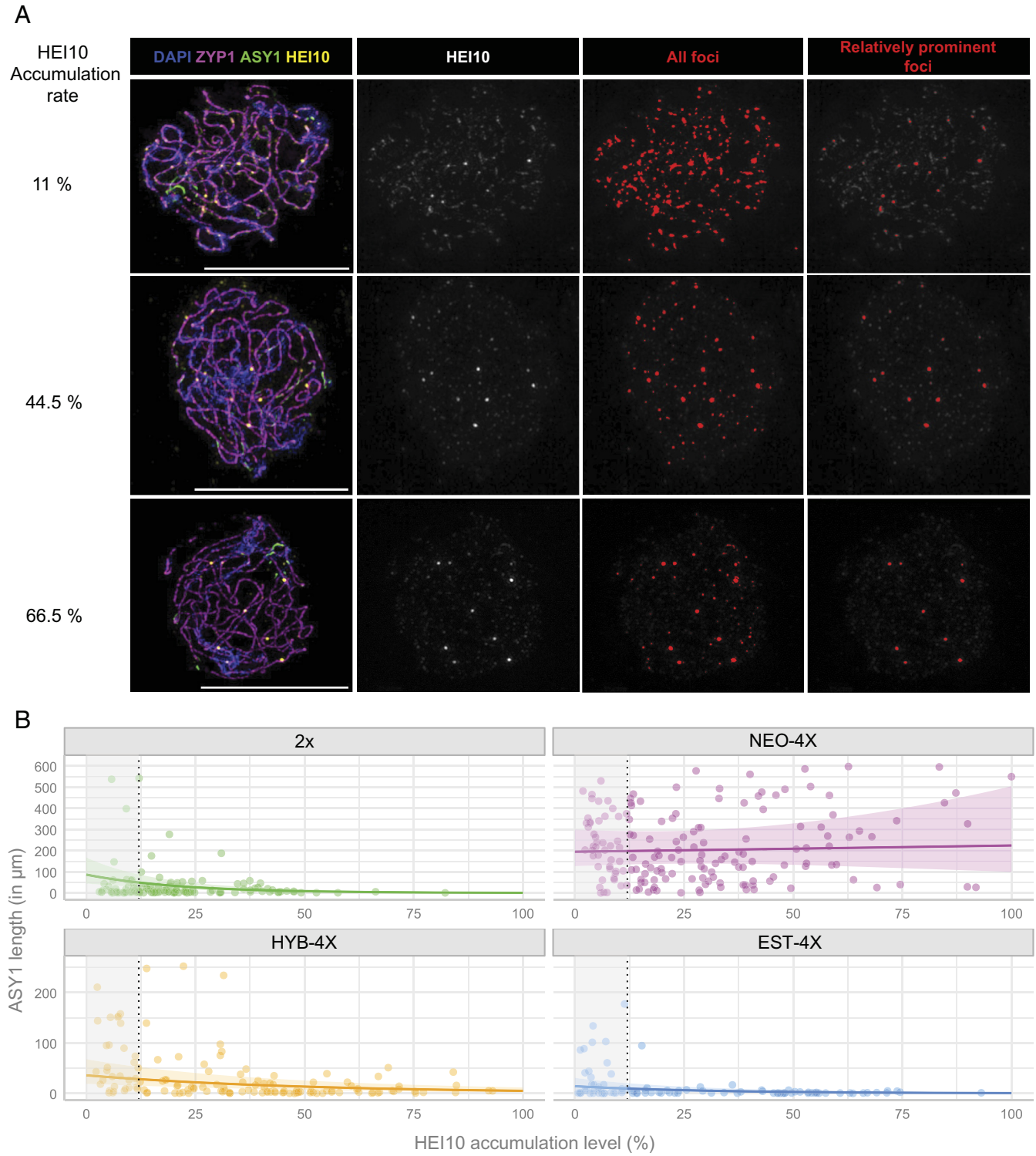

Fig. 2. Modeling synapsis dynamics. (Scale bar, 10 µm.) (*A*) Examples of imaged cells where two different thresholds (highlighted in red) were applied to the HEI10 channel to detect the total signal and prominent foci. Based on the percentage of signal in prominent foci compared to the total, the "HEI10 accumulation level" shown at *Left* was calculated (see also *SI Appendix*, Figs. S2*B*, S13, and S14). (*B*) Plots of all analyzed cells showing HEI10 accumulation level (x-axis) by µm of ASY1 (asynapsis, in the y-axis). Trendlines and 95% CI (shaded areas) are based on estimations from GLMM. The gray-shadowed region in each graph marks data points that were not included in GLMM analysis because they were below the HEI10 accumulation cutoff (12%) we estimated as our detection confidence threshold.

(explanatory variables) for the extent of asynapsis as the response variable (Fig. 2*B* and Dataset S7). GLMMs are especially recommended when data from different individuals (with different sample sizes each) are pooled to deal with pseudoreplication. This is particularly important in heterozygous outcrossing species like *A. arenosa*, which have extensive genetic and phenotypic variation among individuals (33). The individual plant is specified as a random effect in the model formula (*SI Appendix*). This model suggests a negative correlation between HEI10 accumulation and extent of asynapsis, described by an exponential decay curve with substantial explanatory power (R^2 = 0.660; see *Material and Methods* and *SI Appendix*). This fits prior descriptions that large HEI10 foci marking crossovers are associated with full synapsis (10, 14, 22–24, 34). Overall, these analyses illustrate the utility

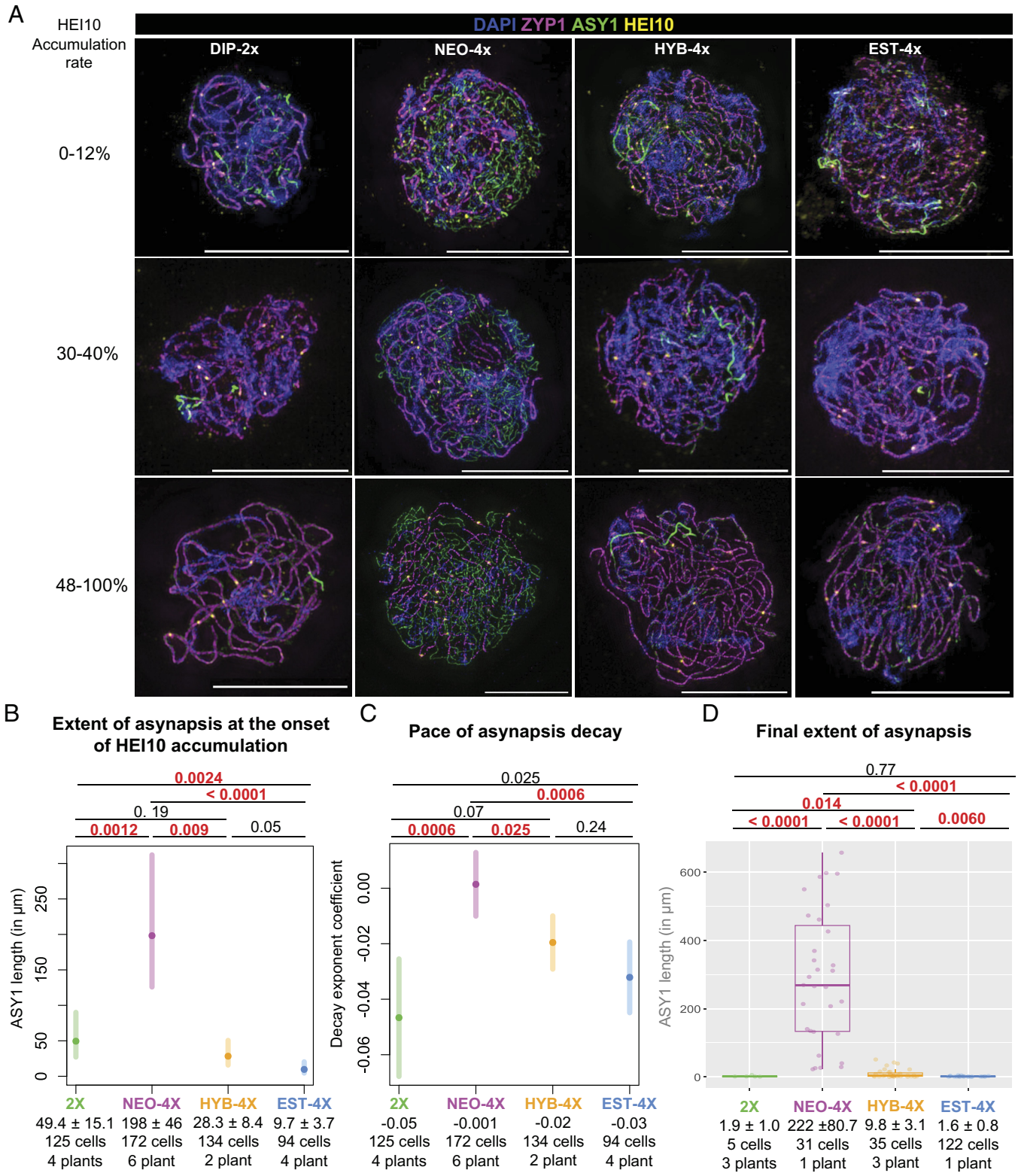

Fig. 3. Differences in synapsis dynamics among genotypes/cytotypes. (Scale bar, 10 µm.) (*A*) Examples of imaged cells of all genotypes with different levels of HEI10 accumulation showing how asynapsis (marked by ASY1, green) generally declines as HEI10 accumulation level increases, except in NEO-4X. Each channel is shown separately, in *SI Appendix*, Figs. S3–S6. (*B*) Plot of the predicted extent of asynapsis by a Gamma-GLMM at the onset of HEI10 accumulation. Error bars represent 95% CI. (*C*) Plot of decay exponent coefficients estimated by a Gamma-GLMM for different genotypes. Error bars represent 95% CI. (*D*) Box plot of the final level of asynapsis, at levels of HEI10 accumulation where synapsis does not progress further. *P*-values are indicated on *Top* of the plots for each comparison (according to Wald's test on Gamma-GLMM coefficients). To better appreciate the scale for 2X, HYB-4X, and EST-4X, *SI Appendix*, Fig. S8 includes solely the results for these genotypes. Significant *P*-values are highlighted in red. Mean values (Mean ± SE) and sample sizes are indicated in the lower part of the plots.

of HEI10 accumulation level as a quantitative marker for developmental progression during mid-prophase I, and as a reference to quantify synapsis dynamics.

Synapsis Stalls in NEO-4X but Is Optimized in EST-4X. Despite the overall negative association between HEI10 accumulation level and the extent of asynapsis, plotting asynapsis (µm of ASY1 signal)

against HEI10 accumulation revealed strong differences among genotypes, particularly for NEO-4X (Fig. 2*B*). Notably, NEO-4X exhibited higher levels of asynapsis at the onset of HEI10 accumulation (which we consider to be at our above-calculated threshold of 12%) and little or no progress afterward, indicated by a flat trend line. To quantitatively analyze the differences in synapsis among genotypes, we examined the predictions and coefficients from our fitted model (Fig. 3 *B*–*D*). We doubled the values of ASY1 length in 2X so they can be directly compared with those of tetraploids. At the onset of HEI10 accumulation (defined as our 12% cutoff), the extent of asynapsis was notably higher in NEO-4X (nearly 200 µm of ASY1; Fig. 3 *A* and *B* and *SI Appendix*, Figs. S3 and S4) compared to 2X (about 50 µm of ASY1). In contrast, EST-4X showed minor asynapsis at this point (less than 10 µm of ASY1), significantly different from both NEO-4X and 2X (Fig. 3 *A* and *B* and *SI Appendix*, Figs. S3, S4 and S6). HYB-4X presented intermediate values (almost 30 µm ASY1; Fig. 3 *A* and *B* and *SI Appendix*, Fig. S5), not significantly different from 2X or EST-4X but differing from NEO-4X. Overall, this analysis demonstrates that asynapsis at the onset of HEI10 accumulation varies significantly across genotypes, with NEO-4X exhibiting the highest levels. Interestingly, EST-4X displayed lower asynapsis than 2X, indicating it has more efficient early synapsis relative to HEI10 accumulation.

The analyses above raised the question whether synapsis in NEO-4X is terminally stalled or merely very slow. Our Gamma-GLMM allowed us to compare the pace of synapsis progression across all genotypes by testing for differences in decay exponent coefficients of ASY1 length relative to HEI10 accumulation levels (Fig. 3*C*). We found statistically comparable decay exponent coefficients in 2X, HYB-4X, and EST-4X (Fig. 3*D*), which are all significantly different from 0 ($P < 0.0001$ for all). This means that ASY1 length changes exponentially as HEI10 accumulation increases. In contrast, the decay exponent of NEO-4X was not significantly different from 0 ($P = 0.8$, Fig. 3 *A* and *D*) and differed significantly from all other genotypes (Fig. 3*D*), hence the flat trendline observed for NEO-4X in Fig. 2*B*. This result suggests that NEO-4X does not significantly increase synapsis as HEI10 accumulation advances, indicating that the extensive asynapsis present at the beginning persists through to the end of pachytene. These findings support the hypothesis that NEO-4X synapsis terminally stalls before HEI10 accumulation begins. Although GLMM analysis excels in dealing with differences between individuals, plotting each plant individually does suggest some differences in behavior (*SI Appendix*, Fig. S7). Therefore, we cannot rule out that some individual plants differ from the overall trend.

We also examined the final levels of asynapsis by determining at what HEI10 accumulation level asynapsis ceases to decline. To do so, we identified the HEI10 accumulation level at which decay exponent coefficients for all genotypes were not significantly different from zero. We found that models including only cells with HEI10 accumulation levels greater than 49% had decay exponent coefficients for all genotypes not significantly different from zero (at least, $P = 0.12$, Gamma-GLMM, $R^2 = 0.849$). This model suggests that at this cutoff, cells have reached their asynapsis minimum. At this HEI10 accumulation level, both 2X and EST-4X had reached full synapsis (less than 2 µm of ASY1, Fig. 3*D* and *SI Appendix*, Figs. S3 and S6). NEO-4X in contrast, retained very high levels of asynapsis (Fig. 3*D* and *SI Appendix*, Fig. S4). HYB-4X showed intermediate levels (almost 10 of µm of ASY1) significantly different from all the other genotypes, suggesting synaptic completion in the tetraploids has an additive or quantitative genetic basis.

Neo-Tetraploids have Weaker Coalignment of Late Asynaptic Regions. Having observed that synapsis stalls in NEO-4X already before HEI10 starts accumulating, we hypothesized asynapsis in NEO-4X may be due to even earlier problems, e.g., during pairing, which leads to coalignment. Thus, we examined coalignment in cells with 30-150 µm of linear ASY1 signals, which allows assessment relative to axis position (this becomes difficult in cells with greater ASY1 lengths). In this subsampled set, we observed two types of geometry: "irregular," where pairs of asynaptic axes are not near one another, and "parallel," where asynaptic axes could be easily observed as coaligned ASY1 signals (Fig. 4 *A* and *B*). These parallel asynaptic structures were typically 0.5 to 10 µm long, and could be seen as either terminal asynaptic regions at chromosome ends, or interstitial bubbles where asynaptic regions lie between two synapsed regions (Fig. 4 *A* and *B*). We believe these asynaptic regions did not have time to synapse yet (or in NEO-4X had stalled) as opposed to arising from e.g., unresolved interlocks, as we did not observe interlocks when these structures were examined in 3D. We scored the number of parallel and irregular structures per cell and used it as a response variable in a Negative-binomial-GLMM (*SI Appendix*, Fig. S9*A*) where ASY1 length was the explanatory variable. We indeed observed (with a substantial explanatory power; $R^2 = 0.7$) that there was a positive correlation between the length of ASY1 and the number of parallel axes. We interrogated this model to ask whether there are differences in the number of parallel axes between genotypes at comparable levels of asynapsis (ASY1 length = 100 microns), and found that NEO-4X has fewer parallel asynaptic axes than the other three genotypes (at most $P < 0.0052$, Negative-binomial-GLMM, Fig. 4*C*).

EST-4X and NEO-4X Show Different Early Synapsis Dynamics. Issues with pairing might also manifest as problems with synaptic initiation and/or elongation (19, 35), so we sought to get more insights into the initiation of synapsis by examining ZYP1 signals in early to mid-zygotene cells with little synapsis. We observed two kinds of ZYP1 signals in these cells: punctate signals, likely corresponding to synapsis initiation sites, and more elongated signals that we interpret as events where the synaptonemal complex has begun to elongate from a previous synapsis initiation site. To better understand the dynamics of ZYP1 signals, we first modeled their number (response variable) as a function of total ZYP1 length (explanatory variable). Although we cannot rule out that some synaptic stretches are reverted, we used the total length of ZYP1 as a proxy of developmental time (the longer the total ZYP1 length, the later the progress). Here, we used Generalized Linear Models (GLM, which differ from GLMM in that it does not control for individual variation or any other random effect) as they showed a better fit to the data than GLMMs (*SI Appendix*).

Although we observed no differences in the behavior of punctate signals (*SI Appendix*, Fig. S9 *B*–*D*), when we modeled the dynamics of the appearance of elongated ones, we fitted a negative-binomial-GLM with very strong explanatory power ($R^2 = 0.98$, Fig. 4*E*), which suggests a linear correlation between the number of elongated signals and the total length of ZYP1. Our GLM analysis showed a greater initial number of elongated ZYP1 signals (the model's intercept) in NEO-4X than EST-4X (Fig. 4*F*). Interestingly, we also observed that the rate at which the number of elongated signals increases as the total ZYP1 length grows (the model's slope) is significantly greater in EST-4X than in NEO-4X. Since we already saw NEO-4X has fewer coaligned regions and does not complete synapsis, we hypothesize that these differences in slope mean that synapsis initiation sites elongate

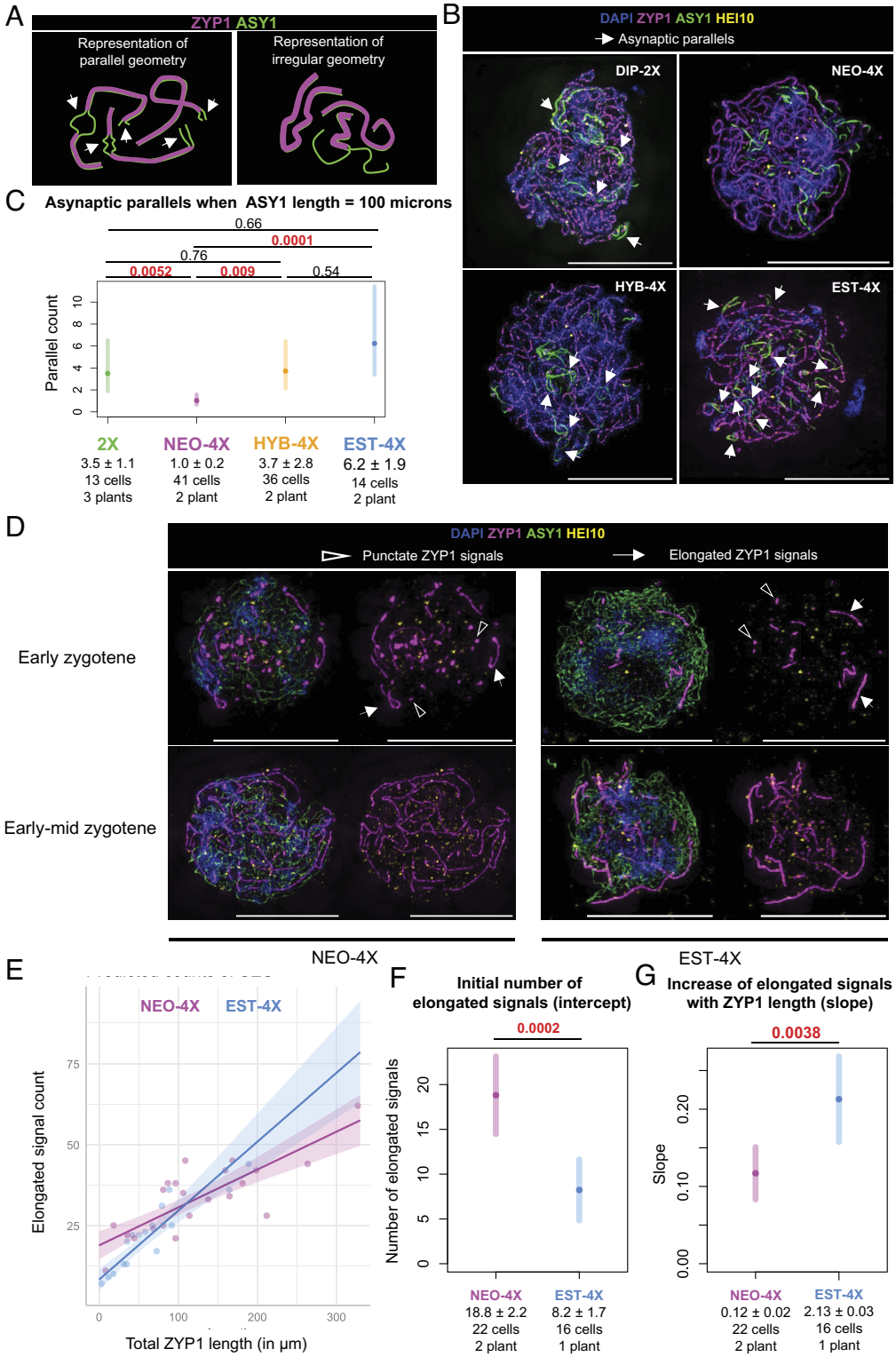

Fig. 4. Early synaptic defects in NEO-4X. (Scale bar, 10 µm.) (*A*) Example illustration of two types of geometry of asynaptic regions observed: parallel and irregular. (*B*) Examples of these structures observed in cells from the four genotypes. Arrowheads indicate regions classified as "parallel." (*C*) GLMM results showing differences in the number of parallels when ASY1 length is 100 µm in all the genotypes, indicating differences in the frequencies of these structures. (*D*) Examples of early and early-to-mid zygotene meiocytes showing punctate (shaded arrowheads) and elongated (white arrowheads) ZYP1 signals. (*E*) Plot of data and predicted trendlines for NEO-4X and EST-4X according to our fitted model (Poisson-GLM) for elongated ZYP1 segments by total ZYP1 length. (*F* and *G*) Plots showing differences predicted by the fitted model in (*F*) the intercept for both genotypes (the initial number of elongated signals, when ZYP1 length is zero) and (*G*) the slope (the increase in the number of elongated signals as ZYP1 length grows). *P*-values are indicated on *Top* of the plots for each comparison (according to Wald's test on Poisson-GLMM coefficients). Significant *P*-values are highlighted in red. Mean values (Mean ± SE) and sample sizes are indicated in the lower part of the plots.

more readily in EST-4X, whereas in NEO-4X synapsis initiates normally, but a lower proportion of the initiation sites are proficient to elongate normally.

Preferential Localization of Prominent HEI10 Foci to Synapsed Regions Is Stage-Dependent. We next asked whether or how HEI10 focus development is affected by the synaptic defects in

NEO-4X by examining HEI10 localization in more detail. It has been shown in other species that HEI10 forms foci at synaptic initiation sites (11, 17, 36–38), thus, we began by analyzing cells in early zygotene, when synapsis is just starting. Irrespective of genotype, in nuclei with incipient synapsis, the few prominent HEI10 foci localize with no apparent preference to either asynaptic axes (which accounts for the vast majority of axes at this stage) or occasionally on the few small ZYP1 signals where synapsis has initiated (early zygotene cells in Fig. 4*D*). This observation is consistent with reports in *Arabidopsis thaliana* at the earliest stages of synapsis (10, 39), but not other species, where HEI10 orthologs are specifically associated with synapsis initiation sites (11, 17, 36, 37). Although, nonprominent foci are more difficult to distinguish from background signal, the lack of preference of prominent foci for synapsed stretches, suggests that in *A. arenosa*, HEI10 only marks (at most) a subset of synapsis initiation sites, and is not a reliable marker for them. In all genotypes, HEI10 is mostly found in discrete punctate foci, though on rare occasions, we observed linear HEI10 signal on unsynapsed chromosomes overlapping with ASY1, resembling a pattern previously described in wheat (24) (*SI Appendix*, Fig. S10). Importantly, we did not consider these cells in the previously described analyses as these linear signals could skew the results.

In more advanced stages, where HEI10 condensation to fewer foci has begun (HEI10 accumulation levels of 12 to 24%), we observed that prominent HEI10 foci are more commonly located on synapsed regions in all genotypes (early-mid zygotene cells in Figs. 4*D* and 5*A*), though they can occasionally also occur on unsynapsed regions at this stage (*SI Appendix*, Fig. S11 *A*–*C*). Later, at 45-100% HEI10 accumulation levels, enlarged discrete foci were found almost exclusively in synapsed regions. This was true for 2X, HYB-4X, and EST-4X meiocytes that are fully or nearly fully synapsed, but also for meiocytes in NEO-4X that still retain extensive asynapsis; only 3 of 919 prominent foci were localized on unsynapsed axes in NEO-4X (Fig. 5*A*). Remarkably, we observed that in these late asynaptic NEO-4X cells, even small tracts of synapsis (<5 μm) can contain a prominent HEI10 focus (Fig. 5 *B* and *C*), resembling observations in mutants with patchy synapsis in *C. elegans* (18, 20) and *A. thaliana* (21, 39).

Extensive Asynapsis Accompanies Elevated Crossover Number. Given that synaptic alterations have been shown to alter crossover number and/or patterning in other species (18–21), we asked whether defective synapsis in NEO-4X is related to their elevated crossover number. Since the three tetraploid genotypes (NEO-4X, HYB-4X, EST-4X) have different levels of asynapsis (Fig. 3) and different crossover numbers (Fig. 1), we tested whether there is a correlation among cells within a cytotype/genotype between degree of asynapsis and crossover number. We filtered for cells where HEI10 foci likely specifically mark crossovers (late pachytene), by determining after what HEI10 accumulation level the number of detected prominent foci most closely resembled the crossover count at diakinesis for that genotype (*SI Appendix*, Fig. S11*D*). This corresponded to HEI10 accumulation levels greater than 44, 59, 48, and 65% for 2X, NEO-4X, HYB-4X, and EST-4X, respectively. Once we calculated the number of HEI10 foci in each late pachytene cell, we used it as a response variable in a Poisson-GLM with the extent of asynapsis (μm of ASY1) as an explanatory variable. Our Poisson-GLM suggested, with substantial explanatory power (R^2 = 0.608), that there is a significant ($P < 0.0001$) logarithmic relationship between the extent of asynapsis and crossover number (Fig. 5*D*). This nonlinear relationship, along with the fact that we found no correlation within genotypes (R^2 = 0.141, at most), suggests that the potential relationship between asynapsis and misregulation of crossovers is complex.

Discussion

We previously showed that appropriate crossover number and patterning can prevent meiotic instability in autopolyploids (26, 29). We previously also reported that the synaptonemal complex is compromised in neo-tetraploids of *Arabidopsis arenosa* (26).

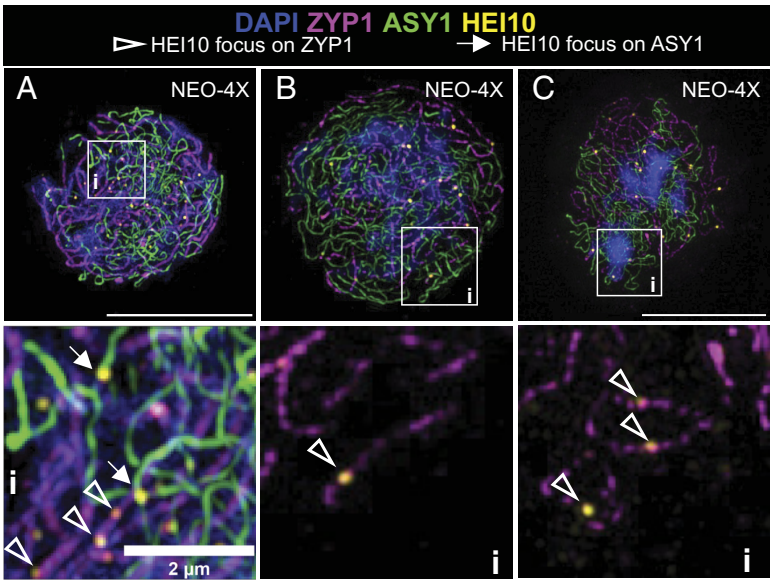

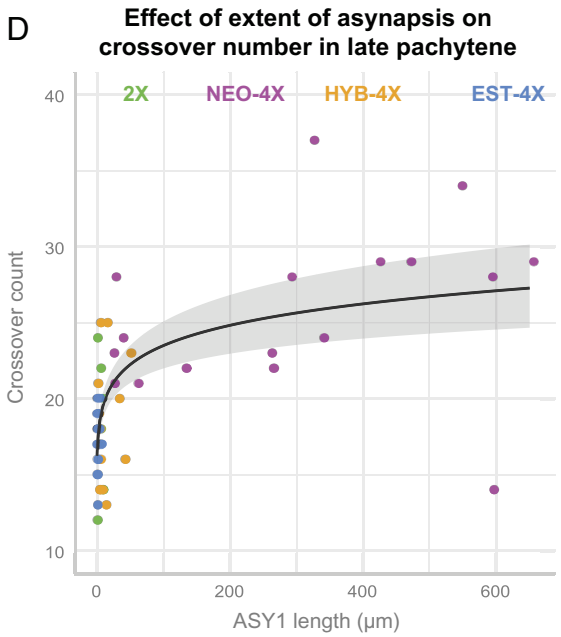

Fig. 5. Relationship of synapsis with HEI10 localization and crossover number. (*A*) An example of a mid-zygotene cell in NEO-4X with prominent HEI10 foci colocalizing with both asynaptic (ASY1) and synapsed (ZYP1) axes. (Ai) Zoomed-in image of the dashed square in (*A*). (*B*) and (*C*), and their respective zoom in details (Bi) and (Ci) show examples of late pachytene-like cells with persisting asynapsis where prominent late HEI10 foci (presumably marking crossovers) specifically localize to synapsed chromosomes (marked by ZYP1). Notably, even short ZYP1 stretches can have late HEI10 foci. (*D*) Plot showing the exponential relationship between extent of asynapsis and crossover number for late pachytene(-like) cells.

Synaptic defects have also been reported in neo-autotetraploid *C. elegans* (40), as well as neo-allopolyploid *A. suecica* (41). Interestingly, established tetraploids of both *A. suecica* and *A. arenosa* exhibit complete synapsis (26, 42), suggesting its reestablishment is important for polyploids. In this study, we thus explored the dynamics of synapsis in both neo- and established tetraploid *A. arenosa* to better understand the origin of the problem itself, and more importantly, to ask whether improving the dynamics of this process might be an important adaptation for meiotic stability in established tetraploids.

Prophase I, the stage where crossover patterning and synapsis take place (6), is a highly dynamic stage of meiosis. Quantitative analysis of a dynamic process like synapsis ideally would involve live imaging experiments (27), but this limits image resolution, and is not tenable in nonmodel systems where appropriate fluorescently tagged lines are not available. Moreover, live imaging requires fluorescent tags, but tagging HEI10, as seen for the *C. elegans* ortholog ZHP-3, can compromise its wild type function (43). An appealing alternative is to measure quantifiable dynamics of one process relative to quantifiable dynamics of another process in images of fixed meiocytes, which also allows analysis using superresolution microscopy. Such an approach has been used to study e.g., the dynamics of DSB repair relative to synapsis progression in *A. thaliana* (44). Here, we further developed this approach to analyze synapsis dynamics using HEI10 progression as a reference (Fig. 6). While informative, this approach does carry the caveat that it provides only relative information and does not measure how long events take in real time.

Recent work in several species has focused on the role that the synaptonemal complex [which links the axes of homologous chromosomes and provides a platform for the maturation and regulation of recombination (45–48)], plays in the final number and pattern of crossovers on chromosomes (47, 49–51). Comparing synaptic progression to the progression of HEI10 accumulation, we found that there are differences among genotypes in synapsis dynamics already from the very beginning of the process (Fig. 6). Our data suggest that synapsis initiation occurs seemingly normally in neo-polyploids but elongates less efficiently in NEO-4X than EST-4X. This may result from defects in homologous axis pairing or synaptonemal complex polymerization. The former is supported based on asynaptic axes being more commonly parallel in 2X, HYB-4X, and EST-4X than in NEO-4X. In late zygotene in NEO-4X, many regions remain unaligned, likely unpaired, which may directly hinder synapsis completion. This diverges somewhat from the conclusions in autotetraploid *C. elegans*, where synaptic defects were observed even when axes were coaligned in groups of four, leading to the idea that homologous chromosomes may "compete for establishing synapsis connections" (40). The same may happen locally in *A. arenosa* as well, where regional coalignment of all four axes has also been observed, but these four-way alignments occur in neo- as well as established polyploids, and thus they seem in themselves to not block synapsis (26). It is nevertheless possible that there are pairing problems arising from competition among the four homologs in neo-polyploids that could hinder synaptonemal complex elongation, while the established polyploids evolved a solution to this challenge. Another explanation for inefficient synapsis in neo-polyploids, could be that extra chromosome sets complicate chromosome movements during prophase I, which are important to promote pairing and synapsis (19, 35, 52). It should be noted that, although the population used to generate neo-tetraploids (SNO) belongs to the closest diploid lineage to the established tetraploids, the extent to which the details may vary among populations remains to be tested.

How might evolved tetraploids have solved the synaptic issues their neo-tetraploid counterparts face? Previously, we identified genes that show evidence of having been targets of natural selection in the established tetraploid *A. arenosa* lineage, including numerous potentially relevant meiosis genes (28, 53–55). If pairing itself is the ultimate problem, a possible candidate for the evolved solution in established tetraploids is *PUTATIVE RECOMBINATION INITIATION DEFECTS 3* (*PRD3)* (56), which shows strong evidence of having been targeted by selection in tetraploid *A. arenosa* (28). *PRD3* encodes a homolog of yeast *Mer2* (57). When Mer2/PRD3 is associated with the axis (58), it is essential for the formation of the DSBs that are required for complete pairing and synapsis nucleation (56, 58, 59) but not initiation (58). Evolved variants of *PRD3* could thus enhance pairing and synapsis nucleation, potentially explaining the different dynamics of appearance of punctate and elongated synaptic stretches between EST-4X and NEO-4X. Functionally testing whether or how evolved *PRD3 alleles* might contribute to an evolved pairing and synapsis in EST-4X background will be interesting to test. DNA strand invasion is a requisite in plants for pairing and synapsis (60, 61) which is regulated antagonistically by SOLO DANCERS (SDS) (56) and FIDGETIN-LIKE-1 INTERACTING PROTEIN (FLIP) (62) (and other factors), and the genes encoding them also show strong evidence of selection in the tetraploid lineage (55). *REDUCED MALE FERTILITY 1* (*RMF1)*, another gene with evidence of having been targeted by selection in *A. arenosa*, was also recently shown to negatively regulate strand invasion (63). We also previously suggested that changes to the chromosome axis (e.g., stiffening), could lead to more efficient chromosome pairing and synapsis in the established tetraploids (26, 33). This would fit with the strong evidence for selection targeting the axis proteins ASY1 and ASYNAPSIS3 (ASY3) in the tetraploid lineage (28, 55), where tetraploid alleles have already been shown to reduce multivalent frequency and

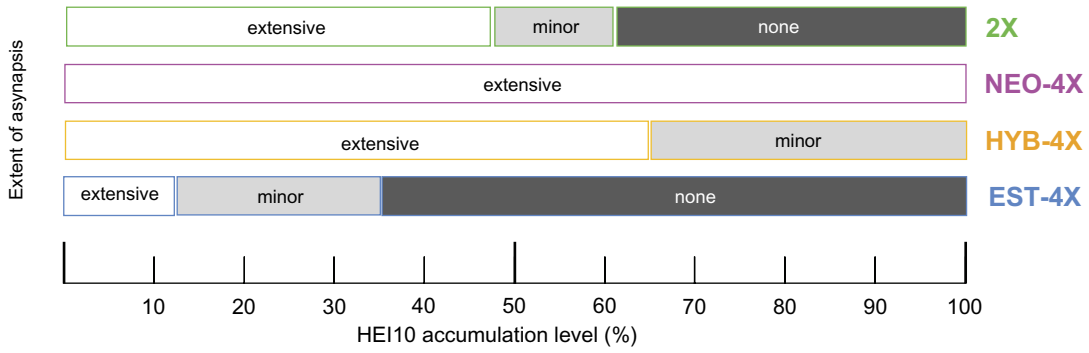

Fig. 6. Genotype-specific timeline of mid-prophase events at the level of HEI10 accumulation and synapsis. The asynapsis categories were established arbitrarily as extensive asynapsis > 10 μm ASY1, minor 5 to 10 μm ASY1, none < 5 μm ASY1.

increase crossover spacing. Moreover, recently, ASY3 dosage has been shown to affect synapsis and crossover number in allotetraploid *Brassica napus* (64). However, genetically generated established tetraploid plants homozygous for diploid alleles of ASY1 and ASY3 do not have defects in synapsis completion, suggesting that while they contribute to crossover patterning, they are not responsible for the difference in synapsis between diploids and tetraploid genotypes (33). Since synapsis appears to be an important defect in neo-tetraploids, it is intriguing that selection also targeted the synaptonemal complex protein ZYP1 (28, 55), suggesting the derived allele found in tetraploids may have a very direct role of modifying the synaptonemal complex itself, perhaps by enhancing the efficiency of polymerization, but this, too, remains to be tested in future work.

An important question regarding the synaptic defects observed in neo-polyploids is whether they relate directly to crossover rate. In neo-tetraploids of *A. arenosa* (26) as well as other species (65, 66), per-chromosome crossover rates increase relative to diploids, but the reason for this has remained unclear. Here, we found a broad correlation across genotypes between the extent of asynapsis and crossover rate, with neo-tetraploids having both strongly defective synapsis as well as higher crossover numbers relative to both established tetraploids and neo-tetraploid/established tetraploid hybrids. We found additional support for this correlation from the finding that asynapsis and crossover number correlate positively across cells. However, the correlation is nonlinear, perhaps indicating that crossover number is not proportional to the extent of asynapsis per se, but maybe to other factors like the number of synaptic patches (as observed in *A. thaliana pachytene checkpoint-2* (*pch2)* mutants (21)). Alternatively, a threshold-like effect could disrupt crossover regulation only above a certain level of asynapsis, perhaps related to a resumption or continuation of DSB formation. Indeed, DSBs are known to increase in situations where homologs fail to engage through synapsis or crossovers in budding yeast and *C. elegans* (46, 67, 68).

We hypothesize the link between asynapsis and crossover number may be caused at least in part by the fact that neo-tetraploids have HEI10 dynamics taking place in the context of abnormal patchy synapsis. This might allow recombination intermediates that would otherwise not develop into crossovers to accumulate sufficient HEI10 (or another pro-crossover factor) to become crossover-fated. Similar alterations of crossover patterning are reported for the *auxin resistant 1* (*axr1)* (39), *pss1* (19) and *pch2* (21) mutants in *A. thaliana* and *syp-1* knock down mutants in *C. elegans* (18, 20) which have patchy synapsis. Because of its preference for associating with synapsed regions, HEI10 accumulates locally to higher concentrations per length of synaptonemal complex when synapsis is patchy, resulting in nearly every synaptic "patch" developing at least one prominent HEI10 focus (19). Importantly, this would imply that local concentration of HEI10 in synapsed regions can alter the fate of at least some recombination intermediates, implying they retain some plasticity and remain sensitive to HEI10 levels.

We suggest that patchy synapsis in neo-tetraploids might similarly locally concentrate HEI10, assuming about the same amount of protein per unit DNA now accumulates on a smaller total amount of synaptonemal complex length. Conversely, in the context of full synapsis (as in the established tetraploids), HEI10 could be siphoned off recombination intermediates that are not irreversibly crossover-fated; in the context of patchy synapsis this may not be possible, allowing HEI10 to be retained on these plastic sites. The HEI10 present on a synaptic patch would accumulate where it can—a crossover-designated site when one is available, a plastic site when not. When this happens in *A. thaliana* patchy synapsis mutants, it does not result in crossover increase, but this is because the number of synaptic patches in these mutants is lower than the wildtype crossover number. However, in *C. elegans,* where in wild type meiosis there is only one crossover per bivalent, mutants with patchy synapsis do show a crossover increase (18, 20). In *A. arenosa* crossover rates per chromosome pair are also low (1.06 and 1.25 crossovers per chromosome pair in EST-4X and 2X, respectively), and the number of synaptic patches in neo-tetraploids is greater than this (26). Overall, the increased efficiency of synapsis we see in the evolved polyploids of *A. arenosa* likely helps prevent excess recombination intermediates taking on crossover fates, and may also help solve other patterning issues (26).

The clear evidence that meiosis genes are under strong selection in tetraploid *A. arenosa*, and the evidence that meiotic stability has improved in evolved versus neo-tetraploid *A. arenosa*, strongly suggests that it is an important aspect of improved fertility in evolved tetraploids. However, it is also clear that nonmeiotic factors like pollen tube growth also have a great impact on neo-polyploid fertility, and clearly also experienced selection (69). This could explain why, although selection is accepted to act on subtle fitness differences, a mild, induced improvement in meiotic stability in *A. thaliana* neo-tetraploids does not drive an obvious improvement in seed set, as we previously observed (29). Overall, these considerations underscore the need to distinguish meiotic from nonmeiotic traits while studying how adaptive evolution stabilizes fertility in tetraploids. Moreover, we need to address in future work, whether meiosis is truly under selection for fertility per se, versus some other aspect that may affect fertility less directly, such as prevention of genomic instability or aneuploidy.

Materials and Methods

Plant Material. We used lab propagated descendants of natural populations of diploid (2X) and autotetraploid (EST-4X) *A. arenosa* from Strečno, Slovakia (SNO, 2X), and TBG Triberg, Germany (TBG, EST-4X) (25, 70). To produce neo-tetraploids (NEO-4X), we treated 2X 14-d-old seedlings in the apical meristem with 0.05% colchicine (Sigma) diluted in sterile water with 0.05% Silwet-77 (Anawa). Neo-tetraploid branches of treated plants were identified in colchicine-derived chimeric plants using flow cytometry. Confirmed tetraploid branches were used both for crosses (to obtain second-generation nonchimeric neo-tetraploids). We did also generate data from different branches of the same plant. For the experiments described here, we used both colchicine-treated and second-generation neo-tetraploids (as indicated in *SI Appendix*, Fig. S1), since our analysis showed no significant differences between them (*SI Appendix*). To generate tetraploid hybrids (HYB-4X), we crossed EST-4X as male with NEO-4X as a female (as described in *SI Appendix*, Fig. S1). All the HYB-4x individuals used for the experiments in this study were F_1 hybrids. We verified the karyotype of second-generation NEO-4X, HYB-4X, and EST-4X plants in meiotic and mitotic spreads and only proceeded to further analyses with confirmed euploids.

For Metaphase I spreads, we used 9 NEO-4X individuals (1 colchicine-treated individual plus 8 individuals from the next generation n = 23 and n = 8 + 25 + 8 + 1 +1 + 35 + 60 + 34 = 172 cells, respectively); 5 HYB-4X individuals (n = 4 + 3 + 4 + 15 = 26 cells); and 6 EST-4X individuals (n = 110 + 35 + 12 + 3 + 74 + 2 = 236 cells). For analyses of HEI10 foci in diakinesis cells, we used 1 DIP-2X individual (n = 106 cells), 1 NEO-4X (1 individual from the next generation, n = 61 cells); 1 HYB-4X individual (n = 186 cells); and 1 EST-4X individual (n = 123 cells). For analyses of codynamics of synapsis and HEI10 accumulation on SIM-imaged zygotene and pachytene cells, we used 4 DIP-2X individuals (n = 35 + 13 + 24 + 53 = 125 cells); 6 NEO-4X individuals (3 colchicine-treated individuals plus 3 individuals from the next generation, n = 19 + 45 + 45 = 109 and n = 8 + 16 + 38 = 62 cells, respectively); 3 HYB-4X individuals (n = 32 + 44 + 58 = 134 cells); and 4 EST-4X individuals (n = 7 + 5 + 70 + 11 = 93 cells). For analyses of dynamics of synapsis initiation on zygotene SIM-imaged cells HEI10 we used 2 NEO-4X individuals (1 colchicine-treated individual plus

1 individual from the next generation, n = 4 and n = 24 cells, respectively) and 1 EST-4X individual (n = 16 cells). For analyses of dynamics of synapsis initiation on zygotene SIM-imaged cells HEI10 we used 2 NEO-4X individuals (1 colchicine-treated individuals plus 1 individual from the next generation, n = 4 and n = 24 cells, respectively) and 1 EST-4X individual (n = 16 cells). For analyses of asynaptic parallels we used 2 NEO-4X individuals (2 colchicine-treated individual plus 2 individuals from the next generation n = 14 + 29 = 43 and n = 1 + 15=16, respectively); 4 HYB-4X individuals (n = 1 + 5 + 20 + 11 = 37 cells); and 3 EST-4X individuals (n = 6 + 7 + 2 = 15 cells).

Metaphase I and Late Prophase I Spreads. We used chromosome spreads of flower buds fixed in 3:1 ethanol:acetic acid at diplotene, diakinesis (immunostaining of HEI10 for crossover quantification), and metaphase I (univalent and quadrivalent counts). We performed spreads following the protocol in ref. 32, with the minor modifications explained in ref. 29. Spreads were visualized and imaged using a Leica Thunder Imager 3D Tissue epifluorescence microscope.

Immunostaining. For HEI10 foci count for crossover quantification in late prophase I cells (diplotene and diakinesis) we followed the protocol in ref. 32, with the same minor modifications explained in ref. 29. We used a primary monoclonal antibody against *A. thaliana* HEI10 (29) and a secondary goat anti-guinea pig Alexa-488 antibody (both at 1:200 dilution). We visualized and imaged immunostained late prophase I cells with a Leica Thunder Imager 3D Tissue epifluorescence microscope. To visualize HEI10 accumulation and the extent of asynapsis in zygotene/pachytene cells, we used 3D SIM following the protocol described in ref. 71. For this immunostaining protocol, we used the following primary antibodies: rabbit polyclonal anti-HEI10, guinea pig monoclonal anti-ZYP1, guinea pig polyclonal anti-ZYP1, guinea pig polyclonal anti-ASY1 (all with 1:500 dilution) and rat polyclonal anti-ASY1 (with 1:1,000 dilution). We used the following secondary antibodies with a 1:200 dilution: goat anti-rabbit Alexa-647, goat anti-rat Alexa-555, goat anti-guinea pig Alexa-488. Cells were imaged using a Deltavision OMX SIM microscope in 3D stacks of 0.125 microns optical section spacing.

Data Generation and Analysis

Image Analysis and Scoring. Multivalent and univalent scoring was performed blindly in randomized metaphase I images. Each metaphase I image was assigned to a "FSESF" class (A, B, C, D, or E), depending on the quality of the spread and the confidence of the count, with A the best and E the least reliable (examples shown in *SI Appendix*, Fig. S12). Scorability class was considered for statistical analyses. Two-channel multi-image files for HEI10 focus count in late prophase I spreads did not allow image randomization. To analyze HEI10 accumulation and the extent of asynapsis in zygotene/pachytene cells, we processed SIM images in 3D stacks using three different ImageJ Fiji macros applied in batch to the full image set. These macros apply different thresholding methods to detect fluorescence signals (72, 73) of HEI10 or ASY1. Macro 1 analyzes HEI10 signal to estimate the number of prominent foci, and the intensity of both prominent foci and total signal (which we used to calculate the HEI10 accumulation level). To determine which foci are considered as prominent, and what is considered as total signal, we used different thresholding methods available in ImageJ Fiji which are based on frequency histograms (i.e. the distribution) of pixel intensities. Importantly, since experimental variability for HEI10 signal between cells is expected, thresholding methods are based on normalized pixel intensities for each image. Therefore, it is relative intensity, rather than absolute intensity, that determines what is considered as signal versus background, and which foci are considered prominent. How macros apply those thresholds is detailed in *SI Appendix*. Macro 2, analyzes ASY1 signal to measure its 3D length (in μm) to estimate the extent of asynapsis. Macro 3 analyzes the signal from both ASY1 and ZYP1 for quality control purposes. Details about the macros are further explained in *SI Appendix*. Raw data scored from each microscopy image are detailed in Datasets S1–S7.

Statistical Analysis. All statistical analyses were performed using Rstudio with the version 4.4.0 of R, and plots were made using ggplot2 (74). To analyze late prophase I HEI10 focus count data, since only one individual per genotype was included, we used the classical statistical tests. Since there was unequal variance, we used Kruskal–Wallis and Dunnett tests (for multiple group comparisons) or *t* test/Mann–Whitney *U* for simple comparisons (depending on whether equal variance criterion is met or not, respectively; details in Dataset S6). For other datasets, since there were always genotypes with more than one individual, we used Generalized Linear Mixed Models, to account for random variation between individuals and prevent pseudoreplication. Occasionally we used Generalized Linear Models (which do not control for variability between individuals), when they showed a better fit than GLMMs (*SI Appendix*). We used Gaussian-GLM(M) or Gamma-GLM(M) (more appropriate for skewed data) for continuous data (such as ASY1 length) and Poisson-GLMM or negative binomial-GLMM for discrete data (such as multivalent/univalent or foci counts). We used the glmmTMB R package (75) to fit models. For each analysis we fitted several models and chose the best fit using the Performance (76) and DHARMa (77) R packages. Details on criteria and procedures to select the best-fit are explained in *SI Appendix* and Datasets S6 and S7. For the best fit GLMM, we estimated means, CI, medians, SE, and *P*-values using the emmeans R package (78) with Holm–Bonferroni correction, based on Wald's tests performed by glmmTMB.

Data, Materials, and Software Availability. Images data have been deposited in ETH Research Collection [DOI: 10.3929/ethz-b-000696798 (79), 10.3929/ethz-b-000696907 (80), 10.3929/ethz-b-000696850 (81), 10.3929/ethz-b-000696797 (82), 10.3929/ethz-b-000696798 (83)].

ACKNOWLEDGMENTS. We thank the entire Bomblies group for scientific discussions, particularly Marinela Dukic for constructive feedback and Tadeas Priklopil for critical reading and guidance on statistics. We are thankful to Sophie Thüring for technical support in preparing metaphase I spreads. We also thank Joiselle B. Fernandes for scientific discussions, critical reading of the manuscript and support in editing. We also thank Tobias Schwarz and ETH ScopeM for technical support with SIM. We thank Chris Franklin for providing some of the antibodies used in this work. This project has received funding from the European Union's Horizon 2020 research and innovation programme under the Marie Sklodowska-Curie (MSC) Grant agreement No 101029732 to A.G., as well as ETH core funds (K.B.).

1. G. S. Roeder, Meiotic chromosomes: It takes two to tango. *Genes Dev.* **11**, 2600–2621 (1997).
2. L. Grandont, E. Jenczewski, A. Lloyd, Meiosis and its deviations in polyploid plants. *Cytogenet. Genome Res.* **14**, 171–184 (2013).
3. A. Gonzalo, All ways lead to Rome–Meiotic stabilization can take many routes in nascent polyploid plants. *Genes (Basel).* **13**, 147 (2022).
4. J. Szostak, T. Orr-Weaver, R. Rothstein, F. Stahl, The double-strand-break repair model for recombination. *Cell* **33**, 25–35 (1983).
5. C. Morgan, A. Nayak, N. Hosoya, G. R. Smith, C. Lambing, "Meiotic chromosome organization and its role in recombination and cancer" in *Current Topics in Developmental Biology*, (Elsevier Inc., ed. 1, 2023), pp. 91–126.
6. D. Zickler, N. Kleckner, Meiotic chromosomes: Integrating structure and function. *Annu. Rev. Genet.* **33**, 603–754 (1999).
7. A. Caryl, S. Armstrong, G. Jones, F. Franklin, A homologue of the yeast HOP1 gene is inactivated in the Arabidopsis meiotic mutant asy1. *Chromosoma* **109**, 62–71 (2000).
8. C. Lambing, P. C. Kuo, A. J. Tock, S. D. Topp, I. R. Henderson, ASY1 acts as a dosage-dependent antagonist of telomere-led recombination and mediates crossover interference in Arabidopsis. *Proc. Natl. Acad. Sci. U.S.A.* **117**, 13647–13658 (2020).
9. J. C. Fung, B. Rockmill, M. Odell, G. S. Roeder, Imposition of crossover interference through the nonrandom distribution of synapsis initiation complexes. *Cell* **116**, 795–802 (2004).

10. L. Chelysheva *et al.*, The Arabidopsis HEI10 is a new ZMM protein related to Zip3. *PLoS Genet.* **8**, e1002799 (2012).
11. A. Reynolds *et al.*, RNF212 is a dosage-sensitive regulator of crossing-over during mammalian meiosis. *Nat. Genet.* **45**, 269–78 (2013).
12. P. A. Ziolkowski *et al.*, Natural variation and dosage of the HEI10 meiotic E3 ligase control Arabidopsis crossover recombination. *Genes Dev.* **31**, 306–317 (2017).
13. A. Gonzalo *et al.*, Reducing MSH4 copy number prevents meiotic crossovers between non-homologous chromosomes in Brassica napus. *Nat. Commun.* **10**, 2354 (2019).
14. C. Morgan *et al.*, Diffusion-mediated HEI10 coarsening can explain meiotic crossover positioning in Arabidopsis. *Nat. Commun.* **12**, 4674 (2021).
15. L. Zhang, W. Stauffer, D. Zwicker, A. F. Dernburg, Crossover patterning through kinase-regulated condensation and coarsening of recombination nodules. bioRxiv [Preprint] (2021), 10.1101/2021.08.26.457865. Accessed 1 October 2024.
16. C. M. Anderson, A. Oke, P. Yam, T. Zhuge, J. C. Fung, Reduced crossover interference and increased ZMM-independent recombination in the absence of Tel1/ATM. *PLoS Genet.* **11**, 1–27 (2015).
17. L. Zhang, E. Espagne, A. De Muyt, D. Zickler, N. E. Kleckner, Interference-mediated synaptonemal complex formation with embedded crossover designation. *Proc. Natl. Acad. Sci. U.S.A.* **111**, E5059–E5068 (2014).
18. D. E. Libuda, S. Uzawa, B. J. Meyer, A. M. Villeneuve, Meiotic chromosome structures constrain and respond to designation of crossover sites. *Nature* **502**, 703–706 (2013).
19. Y. Duroc *et al.*, The kinesin AtPSS1 promotes synapsis and is required for proper crossover distribution in Meiosis. *PLoS Genet.* **10**, e1004674 (2014).
20. C. K. Cahoon, J. M. Helm, D. E. Libuda, Synaptonemal complex central region proteins promote localization of pro-crossover factors to recombination events during Caenorhabditis elegans Meiosis. *Genetics* **213**, 395–409 (2019).
21. J. A. Fozard, C. Morgan, M. Howard, Coarsening dynamics can explain meiotic crossover patterning in both the presence and absence of the synaptonemal complex. *eLife* **12**, 1–25 (2023).
22. K. Wang *et al.*, The role of rice HEI10 in the formation of meiotic crossovers. *PLoS Genet.* **8**, e1002809 (2012).
23. L. Grandont *et al.*, Homoeologous chromosome sorting and progression of meiotic recombination in brassica napus: Ploidy does matter!. *Plant Cell* **26**, 1448–1463 (2014).
24. S. D. Desjardins *et al.*, MutS homologue 4 and MutS homologue 5 maintain the obligate crossover in wheat despite stepwise gene loss following polyploidization. *Plant Physiol.* **183**, 1545–1558 (2020).
25. B. Arnold, S.-T. Kim, K. Bomblies, Single geographic origin of a widespread autotetraploid Arabidopsis arenosa lineage followed by interploidy admixture. *Mol. Biol. Evol.* **32**, 1382–1395 (2015).
26. C. Morgan *et al.*, Evolution of crossover interference enables stable autopolyploidy by ensuring pairwise partner connections in Arabidopsis arenosa. *Curr. Biol.* **31**, 4713–4726.e4 (2021).
27. M. A. Prusicki *et al.*, Live cell imaging of meiosis in arabidopsis thaliana. *eLife* **8**, 1–31 (2019).
28. L. Yant *et al.*, Meiotic adaptation to genome duplication in Arabidopsis arenosa. *Curr. Biol.* **23**, 2151–2156 (2013).
29. A. Gonzalo, P. Parra-Nunez, A. L. Bachmann, E. Sanchez-Moran, K. Bomblies, Partial cytological diploidization of neoautotetraploid meiosis by induced cross-over rate reduction. *Proc. Natl. Acad. Sci. U.S.A.* **120**, 2017 (2023).
30. K. Bomblies, G. Jones, C. Franklin, D. Zickler, N. Kleckner, The challenge of evolving stable polyploidy: Could an increase in "crossover interference distance" play a central role? *Chromosoma* **125**, 287–300 (2016).
31. D. Kostoff, Fertility and chromosome length. *J. Hered.* **31**, 33–34 (1940).
32. L. Chelysheva, L. Grandont, M. Grelon, Immunolocalization of meiotic proteins in Brassicaceae: Method 1. *Methods Mol. Biol.* **990**, 93 (2013).
33. C. Morgan, H. Zhang, C. E. Henry, C. F. H. Franklin, K. Bomblies, Derived alleles of two axis proteins affect meiotic traits in autotetraploid Arabidopsis arenosa. *Proc. Natl. Acad. Sci. U.S.A.* **117**, 8980–8988 (2020).
34. M. Ito *et al.*, Distinct and interdependent functions of three RING proteins regulate recombination during mammalian meiosis. bioRxiv [Preprint] (2023), 10.1101/2023.11.07.56609. Accessed 1 October 2024.
35. J. Varas *et al.*, Absence of SUN1 and SUN2 proteins in Arabidopsis thaliana leads to a delay in meiotic progression and defects in synapsis and recombination. *Plant J.* **81**, 329–346 (2015).
36. M. Castellani *et al.*, Meiotic recombination dynamics in plants with repeat-based holocentromeres shed light on the primary drivers of crossover patterning. *Nat. Plants* **10**, 423–438 (2024).
37. S. Agarwal, G. S. Roeder, Zip3 provides a link between recombination enzymes and synaptonemal complex. *Proteins.* **102**, 245–255 (2000).
38. N. Bhalla, D. J. Wynne, V. Jantsch, A. F. Dernburg, ZHP-3 acts at crossovers to couple meiotic recombination with synaptonemal complex disassembly and bivalent formation in C. elegans. *PLoS Genet.* **4**, e1000235 (2008).
39. M. T. Jahns *et al.*, Crossover localisation is regulated by the neddylation posttranslational regulatory pathway. *PLoS Biol.* **12**, e10001930 (2014).
40. S. Mlynarczyk-Evans, B. Roelens, A. M. Villeneuve, Evidence that masking of synapsis imperfections counterbalances quality control to promote efficient meiosis. *PLoS Genet.* **9**, 14–16 (2013).
41. C. Nibau, A. Evans, H. King, D. W. Phillips, A. Lloyd, Homoeologous crossovers are distally biased and underlie genomic instability in first-generation neo-allopolyploid Arabidopsis suecica. *New Phytol.* **244**, 1315–1327 (2024), 10.1111/nph.20095.
42. C. Nibau *et al.*, Meiosis in allopolyploid Arabidopsis suecica. *Plant J.* **111**, 1110–1122 (2022).
43. L. von Diezmann, C. Bristow, O. Rog, Diffusion within the synaptonemal complex can account for signal transduction along meiotic chromosomes. bioRxiv [Preprint] (2024), 10.1101/2024.05.22.595404. Accessed 1 October 2024.
44. M. Martinez-Garcia, C. I. White, F. C. H. Franklin, E. Sanchez-Moran, The role of topoisomerase II in DNA repair and recombination in arabidopsis thaliana. *Int. J. Mol. Sci.* **22**, 13115 (2021).
45. K. Voelkel-meiman, C. Johnston, Y. Thappeta, Separable crossover-promoting and crossover-constraining aspects of Zip1 activity during budding yeast Meiosis. *PLoS Genet.* **5**, 1–39 (2015).
46. X. Mu, H. Murakami, N. Mohibullah, S. Keeney, Chromosome–autonomous feedback down-regulates meiotic DNA break competence upon synaptonemal complex formation. *Genes Dev.* **34**, 1605–1618 (2020).
47. S. G. Gordon, L. E. Kursel, K. Xu, O. Rog, Synaptonemal complex dimerization regulates chromosome alignment and crossover patterning in meiosis. *PLoS Genet.* **17**, e1009205 (2021).
48. L. I. Láscarez-Lagunas *et al.*, ATM/ATR kinases link the synaptonemal complex and DNA double-strand break repair pathway choice. *Curr. Biol.* **32**, 4719–4726.e4 (2022).
49. L. Capilla-Pérez *et al.*, The synaptonemal complex imposes crossover interference and heterochiasmy in Arabidopsis. *Proc. Natl. Acad. Sci. U.S.A.* **118**, 1–11 (2021).
50. M. G. France *et al.*, ZYP1 is required for obligate cross-over formation and cross-over interference in Arabidopsis. *Proc. Natl. Acad. Sci. U.S.A.* **118**, 1–11 (2021).
51. N. Vrielynck *et al.*, SCEP1 and SCEP2 are two new components of the synaptonemal complex central element. *Nat. Plants* **9**, 2016–2030 (2023).
52. L. Cromer *et al.*, Rapid meiotic prophase chromosome movements in Arabidopsis thaliana are linked to essential reorganization at the nuclear envelope. *Nat. Commun.* **15**, 5964 (2024).
53. J. D. Hollister *et al.*, Genetic adaptation associated with genome-doubling in autotetraploid Arabidopsis arenosa. *PLoS Genet* **8**, e1003093 (2012).
54. K. M. Wright *et al.*, Selection on Meiosis genes in diploid and tetraploid Arabidopsis arenosa. *Mol. Biol. Evol.* **32**, 944–955 (2014).
55. M. Bohutínská *et al.*, De novo mutation and rapid protein (co-)evolution during meiotic adaptation in Arabidopsis arenosa. *Mol. Biol. Evol.* **38**, 1980–1994 (2021).
56. A. De Muyt *et al.*, A high throughput genetic screen identifies new early meiotic recombination functions in Arabidopsis thaliana. *PLoS Genet.* **5**, e1000654 (2009).
57. S. Tessé *et al.*, Asy2/Mer2: An evolutionarily conserved mediator of meiotic recombination, pairing, and global chromosome compaction. *Genes Dev.* **31**, 1880–1893 (2017).
58. C. Lambing *et al.*, Differentiated function and localisation of SPO11-1 and PRD3 on the chromosome axis during meiotic DSB formation in Arabidopsis thaliana. *PLoS Genet.* **18**, 1–27 (2022).
59. M. Grelon, D. Vezon, G. Gendrot, G. Pelletier, AtSPO11-1 is necessary for efficient meiotic recombination in plants. *EMBO J.* **20**, 589–600 (2001).
60. F. Couteau *et al.*, Random chromosome segregation without meiotic arrest in both male and female meiocytes of a dmc1 mutant of Arabidopsis. *Plant Cell* **11**, 1623–1634 (1999).
61. C. Oliver, J. L. Santos, M. Pradillo, On the role of some ARGONAUTE proteins in meiosis and DNA repair in Arabidopsis thaliana. *Front. Plant Sci.* **5**, 177 (2014).
62. J. B. Fernandes *et al.*, FIGL1 and its novel partner FLIP form a conserved complex that regulates homologous recombination. *PLoS Genet.* **14**, e1007317 (2018).
63. W. Xu *et al.*, SCFRMF mediates degradation of the meiosis-specific recombinase DMC1. *Nat. Commun.* **14**, 5044 (2023).
64. L. Chu *et al.*, ASYNAPSIS3 has diverse dosage-dependent effects on meiotic crossover formation in Brassica napus. *Plant Cell* **36**, 3838–3856 (2024).
65. M. Leflon *et al.*, Crossovers get a boost in brassica allotriploid and allotetraploid hybrids. *Plant Cell* **22**, 2253–2264 (2010).
66. A. Pecinka, W. Fang, M. Rehmsmeier, A. Levy, O. Mittelsten Scheid, Polyploidization increases meiotic recombination frequency in Arabidopsis. *BMC Biol.* **9**, 24 (2011).
67. E. L. Stamper *et al.*, Identification of dsb-1, a protein required for initiation of meiotic recombination in caenorhabditis elegans, illuminates a crossover assurance checkpoint. *PLoS Genet.* **9**, 1–18 (2013).
68. D. Thacker, N. Mohibullah, X. Zhu, S. Keeney, Homologue engagement controls meiotic DNA break number and distribution. *Nature* **510**, 241–246 (2014).
69. J. Westermann, T. Srikant, A. Gonzalo, H. S. Tan, K. Bomblies, Defective pollen tube tip growth induces neo-polyploid infertility. *Science* **383**, eadh0755 (2024).
70. S. Marburger *et al.*, Interspecific introgression mediates adaptation to whole genome duplication. *Nat. Commun.* **10**, 5218 (2019).
71. C. Morgan, E. Wegel, Cytological characterization of Arabidopsis arenosa polyploids by SIM. *Methods Mol. Biol.* **2061**, 37–46 (2020).
72. J. C. Yen, F. J. Chang, S. Chang, A new criterion for automatic multilevel thresholding. *IEEE Trans. Image Process.* **4**, 370–378 (1995).
73. W. H. Tsai, Moment-preserving thresholding: A new approach. *Comput. Vision, Graph. Image Process.* **29**, 377–393 (1985).
74. H. Wickham, Elegant graphics for data analysis. https://ggplot2.tidyverse.org (2016). Accessed 1 October 2024.
75. M.E. Brooks *et al.*, glmmTMB balances speed and flexibility among packages for zero-inflated generalized linear mixed modeling. *R J.* **9**, 378 (2017).
76. D. Lüdecke, M. Ben-Shachar, I. Patil, P. Waggoner, D. Makowski, Performance: An R package for assessment, comparison and testing of statistical models. *J. Open Source Softw.* **6**, 3139 (2021).
77. F. Hartig, DHARMa: Residual Diagnostics for Hierarchical (Multi-Level/Mixed) Regression Models. http://florianhartig.github.io/DHARMa/ (2022). Accessed 1 October 2024.
78. R. V. Lenth, emmeans: Estimated marginal means, aka least-squares means. https://rvlenth.github.io/emmeans/ (2024). Accessed 1 October 2024.
79. A. Gonzalo, K. Bomblies, Synapsis dynamics in A. arenosa (I) Epifluorescence microscopy. ETH Research Collection. https://doi.org/10.3929/ethz-b-000696796. Deposited 22 October 2024.
80. A. Gonzalo, K. Bomblies, Synapsis dynamics in A. arenosa (II) SIM in NEO-4X. ETH Research Collection. https://doi.org/10.3929/ethz-b-000696907. Deposited 10 October 2024.
81. A. Gonzalo, K. Bomblies, Synapsis dynamics in A. arenosa (III) SIM in HYB-4X. ETH Research Collection. https://doi.org/10.3929/ethz-b-000696850. Deposited 1 November 2024.
82. A. Gonzalo, K. Bomblies, Synapsis dynamics in A. arenosa (IV) SIM in EST-4X. ETH Research Collection. https://doi.org/10.3929/ethz-b-000696797. Deposited 10 October 2024.
83. A. Gonzalo, K. Bomblies, Synapsis dynamics in *A. arenosa* (V) Epifluorescence microscopy. ETH Research Collection. https://doi.org/10.3929/ethz-b-000696798. Deposited 10 October 2024.